

Simulation Studies for Non Invasive Classification of Ischemic and Hemorrhagic Stroke using Near Infrared Spectroscopy

Dalchand Ahirwar¹, Kshitij Shakya¹, Aihik Banerjee², Dheeraj Khurana³ and Shubhajit Roy Chowdhury¹

¹*Biomedical Systems Laboratory, Multimedia Analytics and Systems Group, School of Computing and Electrical Engineering, Indian Institute of Technology, Mandi, India*

²*Department of Biotechnology, Heritage Institute of Technology, Kolkata, India*

³*Department of Neurology, Post Graduate Institute of Medical Education and Research, Chandigarh, India*

Keywords: Ischemic Stroke, Hemorrhagic Stroke, Mid-cerebral Artery, Cerebral Oxygenation Level, Near Infrared Spectroscopy.

Abstract: This paper presents an approach to identify and classify the type of stroke, viz ischemic and hemorrhagic conditions. Ischemic stroke is caused by the blood clot and plaque present in the blood vessel. Hemorrhagic stroke, on the other hand, occurs when a rupture happens in the cerebrovascular artery or mid-cerebral artery causing impairments in blood flow and hence the supply of oxygen to the cerebral tissues. The current research analyses the blood flow velocity, the pressure profile of blood clot and plaque, and the condition at which ischemic and hemorrhagic stroke occurs. Simulation studies show the pressure on the blood vessel walls under ischemic and hemorrhagic stroke conditions and also that under nominal blood flow velocity the hemorrhage does not occur, but when the velocity is sufficient enough to increase the pressure on the wall, rupture of the mid-cerebral artery takes place. The simulation assumes the blood flow to be laminar, non-Newtonian, viscous, incompressible, and the arterial wall as elastic. Using the simulation model, an approach to classifying ischemic and hemorrhagic stroke using near infrared spectroscopy has been proposed in the paper.

1 INTRODUCTION

Stroke is one of the leading causes of mortality and disability worldwide. It is devastating not only for the survivors but also for the caregivers. Globally, the incidence rate of stroke is not only high but also continuously increasing due to the ageing population and intense social pressure. The Indian stroke scenario is no less grim with a comparatively higher rate of incidence and prevalence owing to poor control of risk factors and a lack of public awareness (Pandian JD et al., 2013).

Stroke-related mortality and morbidity in India are higher than they should have been mainly due to the unavailability and the unaffordability of quality stroke management facilities in many parts of the country, especially in the rural areas (Kamalakannan S et al., 2017). Also, speed is of the utmost essence in ensuring the favorable clinical outcome of stroke patients. This necessitates rapid stroke diagnosis modalities (Banerjee TK and Das SK, 2016). Stroke can be broadly classified into two major categories: ischemic

stroke, with around 85- 87 % incidence rate, and hemorrhagic stroke, with around 13-15 % incidence rate (Donnan GA et al., 2008).

Ischemic cerebrovascular accident results from a lack of sufficient blood flow to the brain due to the formation of a clot, whereby the brain is unable to meet its metabolic demands (Radic B, 2017). The consequent deprivation of oxygen and nutrient supply to the brain leads to the death of brain tissues, thereby rendering parts of the brain non-functional or poorly functional (Radic B, 2017).

Hemorrhagic cerebrovascular accident occurs due to a ruptured cerebral blood vessel and the resultant bleeding into the head, whereby the brain is damaged by the impairments in blood flow due to rupture of blood vessel, which is basically bleeding outside of the brain tissue, precisely between the arachnoid mater and pia mater, into the cerebrospinal fluid containing sulci, fissures, and cisterns. Although significantly less common compared to the ischemic stroke, hemorrhagic stroke is associated with a much higher rate of morbidity and mortality (Salonen JT and

Salonen R, 1991).

The current research attempts to explore the mid-cerebral artery, with an objective of finding out the condition for ischemic and hemorrhagic stroke. An approach to classifying ischemic and hemorrhagic stroke using cerebral oxygenation level based on near infrared spectroscopy (NIRS) has been presented. The paper is organized into the following sections. Section II describes the simulation model for mid-cerebral artery, where an ischemic or hemorrhagic stroke is likely to occur. Section III presents the modeling of blood flow through the artery. Section IV presents results and discussion. Section V presents the classification of ischemic and hemorrhagic stroke using NIRS.

2 MODELLING OF MIDDLE CEREBRAL ARTERY

The current work involves simulation studies of the mid-cerebral artery which form the key parameter needed to classify between ischemic and hemorrhagic stroke. The geometry consists of a cylindrically shaped structure of 6mm radius and 50 mm length which has been considered to model the artery. To design an initial blood clot, a sphere of 3 mm radius has been embedded on the upper wall of the artery. To model the blood flow through the cylinder, the artery was assumed to have a 3D laminar flow and to study the effect of blood flow on the wall, solid mechanics accompanied by a stationary study has been used.

This model contains three domains and two primitive points. One domain forms the cylinder containing walls of the artery, second forms the space where blood flows, and third for the blood clot. Two points are arbitrarily constructed to measure pressure on the inner walls of the artery.

Material properties used for simulations are shown in Table I (Garje et al., 2015). The flow under laminar regime was modelled with the no-slip boundary condition, and the blood flow velocity has been assumed with a nominal value of 0.169 m/s.

For the simulation, a hollow cylinder has been assumed, which can be viewed as blood vessel, the space inside the cylinder is modelled as the channel for blood flow, and a spherical shape as a blood clot embedded on the inner side of the cylinder. The initial radius of the sphere was 3 mm and was incremented to increase the range of blockage.

The thickness of artery has been taken as 1 mm with 7 mm radius and 50 mm length. The inlet blood flow velocity has been taken as 0.169 m/s throughout the

Table 1: Material properties used for simulation.

Properties	Blood	Artery	Blood clot
Density (Kg/m ³)	1060	1060	1080
Dynamic viscosity (Pa-s)	0.005	-	-
Poisson's ratio	-	0.49	0.3
Young's Modulus (Pa)	-	2x10 ⁶	6.9x10 ³

simulation.

A finite element mesh has been created for the described geometry with free tetrahedral and fluid dynamic physics for the blood flow channel, and free tetrahedral and general physics for the remaining geometry with number of vertex elements being 25, number of edge elements being 708, number of boundary elements being 12704 and number of elements being 96586.

3 MODELLING THE FLOW OF BLOOD THROUGH THE ARTERY

Let us consider an elastic cylinder as a part of the artery in which a non-Newtonian fluid is flowing and following the power-law (J. Mazumdar, 1992).

The flow rate Q will be given by

$$Q = K a_0^s [g(a_1) - g(a_2)] \quad (1)$$

Where

$$K = \frac{n\pi}{n_0(3n+1)L}$$

$$s = \frac{2n+1}{n}, \quad 0 < n < 1$$

$$n_0 = 2\mu^{\frac{1}{n}}$$

$$g(a) = \frac{t_1 a^s}{s} + t_2 \left[\frac{4a^{s+5}}{s+5} - \frac{15a^{s+4}}{s+4} + \frac{20a^{s+3}}{s+3} - \frac{10a^{s+2}}{s+2} + \frac{a^s}{s} \right]$$

a1 and a2 are the radii which vary corresponding to the pressure exerted at these points.

Despite the obstruction in the path of blood flow, the heart works more to maintain the flow rate, hence

$$Q_1 = Q_2 \tag{2}$$

From equation 1 and 2,

$$k_1 a_{01}^s \Delta p_1 = k_2 a_{02}^s \Delta p_2 \tag{3}$$

$$\frac{\Delta p_1}{\Delta p_2} = \frac{k_2 a_{02}^s}{k_1 a_{01}^s}$$

Where Δp_1 and Δp_2 correspond to the change in $g(a_1)$ and $g(a_2)$, hence it can be concluded that change in radius of the artery corresponds to the pressure change across the artery.

To obtain the cerebral oxygenation level of blood, we focus on the Modified Beer Lamberts law which determines the change in optical density against the absorption of near infrared radiation in blood. The equation for optical density is given by

$$\Delta OD = -\log_{10} \left[\frac{I(t_1, \lambda)}{I(t_0, \lambda)} \right] \tag{4}$$

$$\begin{aligned} &= \sum e_F(\lambda) \Delta c_F DPF(\lambda) d + e_b(\lambda) \Delta c_b DPF(\lambda) d \\ &\quad - \log_{10} \left[\frac{I(t_1, \lambda)}{I(t_0, \lambda)} \right] - \sum e_F(\lambda) \Delta c_F DPF(\lambda) d = e_b(\lambda) \Delta c_b DPF(\lambda) d \\ &\frac{-\log_{10} \left[\frac{I(t_1, \lambda)}{I(t_0, \lambda)} \right] - \sum e_F(\lambda) \Delta c_F DPF(\lambda) d}{e_b(\lambda) DPF(\lambda) d} = \Delta c_b \end{aligned} \tag{5}$$

Where e_F and Δc_F are the extinction coefficient and change in chromophore concentration for chromophores other than oxygenated haemoglobin, respectively. And $e_b(\lambda)$ and Δc_b are the extinction coefficient and change in chromophore concentration for the oxygenated haemoglobin, respectively. Thus equation 5 gives the change in chromophore concentration of oxygenated hemoglobin which is responsible for the cerebral oxygenation in blood. Thus Δc_b will be directly proportional to Q , the volumetric flow rate.

4 SIMULATION RESULTS AND DISCUSSION

4.1 Simulation Results of Modeling of Blood Clot Formation in Mid-cerebral Artery

The artery with initial blood clot of 3 mm radius is shown in Figure 1 with its velocity profile. The results are noted for increasing radius of the blood clot in the order of 0.5 mm, and finally, the blood clot of 6 mm which completely blocks the artery as shown in Figure 2.

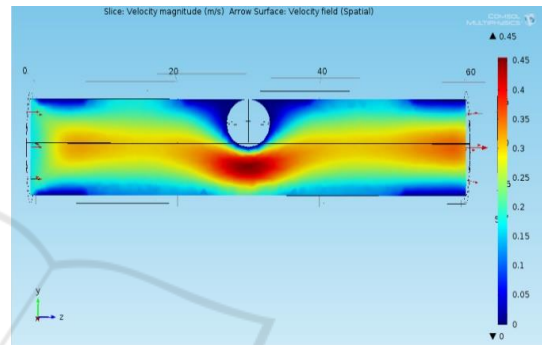


Figure 1: Velocity profile with blood clot of 3mm radius.

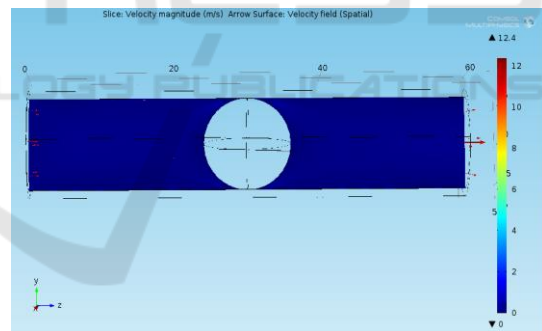


Figure 2: Velocity profile of 6mm radius blood clot.

Figure 3 and 4 show the profile of pressure caused by the blood clot when kept at 3 mm radius and 6 mm radius, respectively. Figure 5 also shows the condition at which ischemia occurs.

The pressure profile at the side walls of the artery is monitored next. Starting from the radius of 3 mm blood clot up to 5.5 mm, the pressure at just above and below the blood clot is shown in Table II. Its corresponding graph is shown in Figure 5.

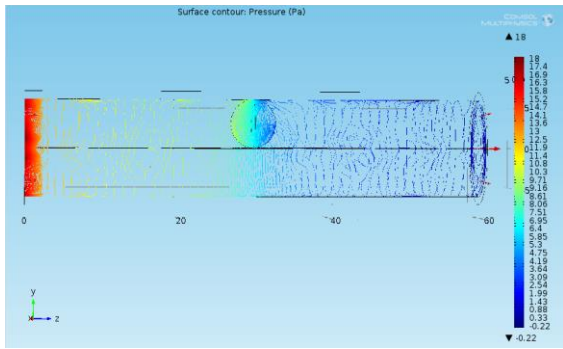


Figure 3: Pressure profile of blood clot at 3 mm radius.

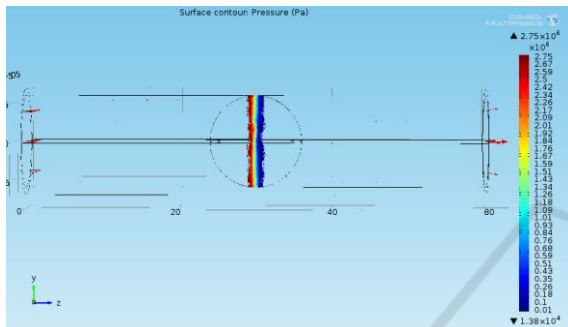


Figure 4: Pressure profile of blood clot at 6 mm radius.

Table 2: Pressure at upper and lower walls of artery.

Radius (mm)	Pressure at Point 1 (Pa)	Pressure at Point 2 (Pa)
3	6.507	6.812
3.5	7.903	7.781
4	10.855	10.910
4.5	16.400	17.711
5	43.388	41.600
5.5	216.090	231.570

Figure 5 and 6 show the expected increase in pressure as the blood clot increases till 5.5 mm. These graphs show that after 91% blockage by the blood clot, the pressure reaches to 216.09 Pa. However, after 100% blockage, that is, at the ischemic condition, the pressure at upper and lower points suddenly rise to 1.37 MPa and 1.39 MPa, respectively.

At this ischemic condition, the blood flow velocity has been increased to observe the pressure increment on the upper and lower walls of the artery and is shown in Table 3 and plotted in Figure 7.

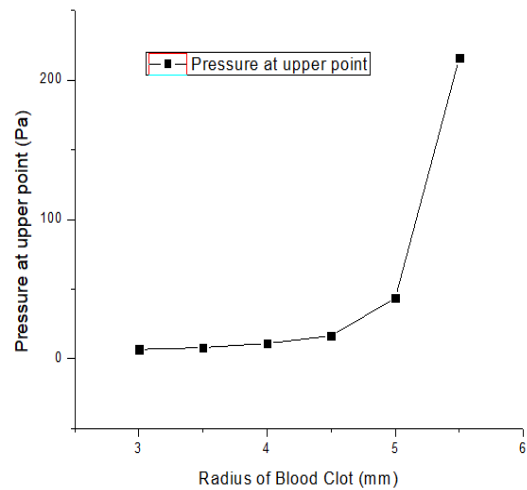


Figure 5: Pressure at upper point of artery wall.

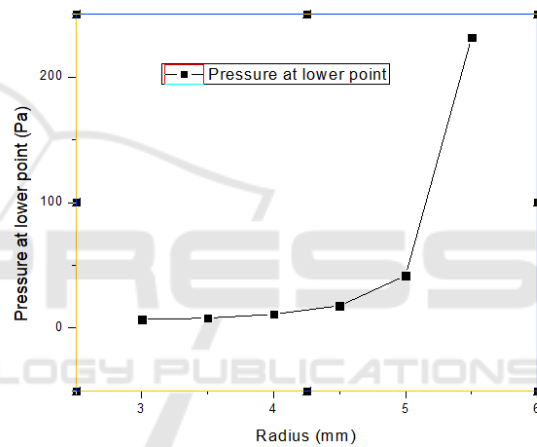


Figure 6: Pressure at lower point of artery wall.

Table 3: Pressure versus velocity at ischemic condition.

Blood flow velocity (m/s)	Pressure at upper wall (MPa)
0.169 (nominal)	1.37
0.18	1.46
0.20	1.62
0.22	1.86
0.24	1.92
0.25	2.005

Table III and Figure 7 show that from nominal blood flow velocity of 0.169 m/s, it takes 0.25 m/s to exceed the wall pressure of 2 MPa, which is the elastic limit of the artery.

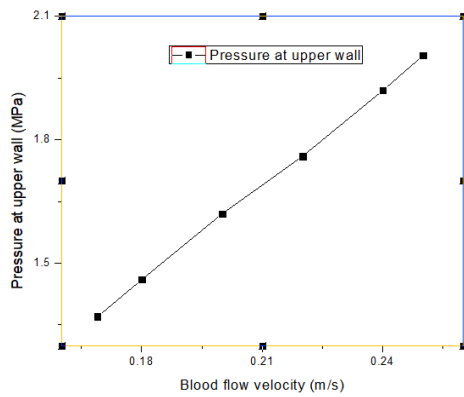


Figure 7: Pressure vs Velocity profile at ischemic condition.

4.2 Simulation of Change in Stiffness of Blood Vessel Due to Fat Accumulation on the Arterial Wall

The change in elasticity on the part of the blood vessel (ring) as a consequence of the accumulation of fat on the inner side of the arterial wall has been studied. The Young’s modulus of the blood vessel and the fat material have been considered as arranged in parallel, and hence the net Young’s modulus of the combination is greater than the ordinary blood vessel, i.e., $2 \times 10^6 \text{ N/m}^2$. The displacement of the ring portion and the stress on that portion has been measured.

Table 4: Relation between blood velocity and stress at two different young’s modulus.

Blood Velocity (m/s)	Stress on Ring when Y=2 MPa	Stress on Ring when Y=11 MPa
0.16	363.12	520.38
0.18	433.17	620.62
0.20	508.91	728.97
0.22	589.97	844.94
0.24	675.51	967.33

Table 5: Relation between blood velocity and displacement at two different young’s modulus.

Blood Velocity (m/s)	Displacement of Ring at Y=2MPa (10^{-4} mm)	Displacement of Ring at Y=11MPa (10^{-4} mm)
0.16	1.11	0.71
0.18	1.32	0.84
0.20	1.56	1.0
0.22	1.81	1.16
0.24	2.08	1.33

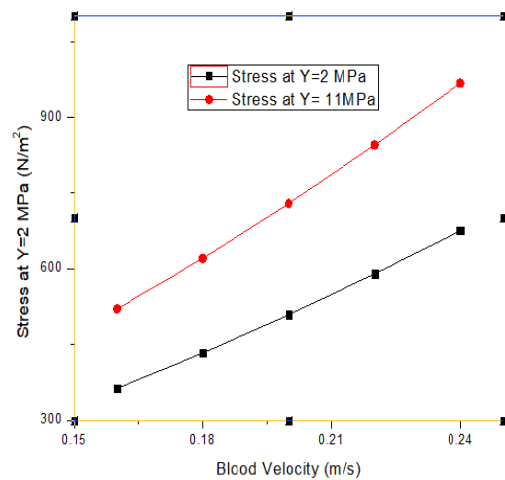


Figure 8: Change in stress due to varying elasticity.

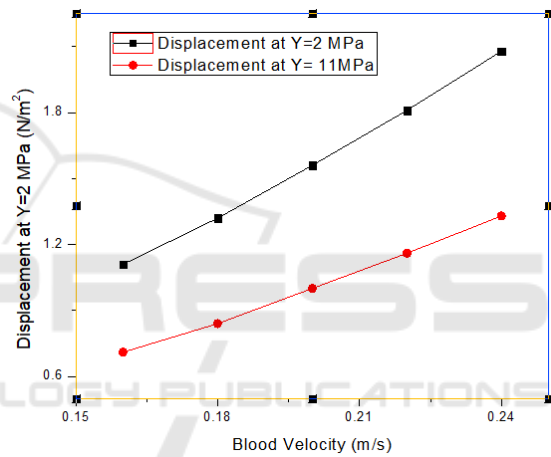


Figure 9: Change in displacement due to varying elasticity.

The relation between the blood flow velocity and the stress for two different Young’s Modulus, one for pure artery and one including a fat layer in parallel has been shown in table IV and plotted in Figure 8. The same for varying displacements has been shown in Table V and Figure 9.

4.3 Simulation Results of Modeling of Hemorrhagic Stroke Condition

The leading cause of hemorrhagic stroke includes hypertension, fat layer deposit, and weakening of blood vessel due to an abnormality in its formation. To design a condition for hemorrhage, the same artery has been taken, and a part of it is assumed to weaken due to the reasons mentioned above. Also assuming a turbulent flow sufficient enough to rupture the weak part of the artery has been modeled in Figure 10, and

its rupture under the hemorrhagic condition is shown in Figure 11.

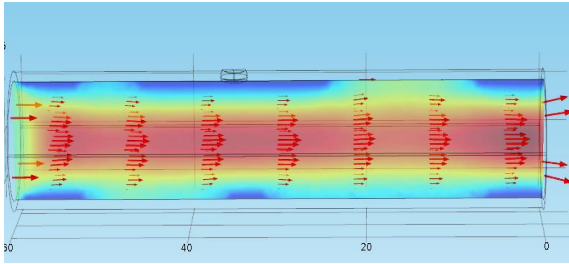


Figure 10: Healthy artery with a weak point.

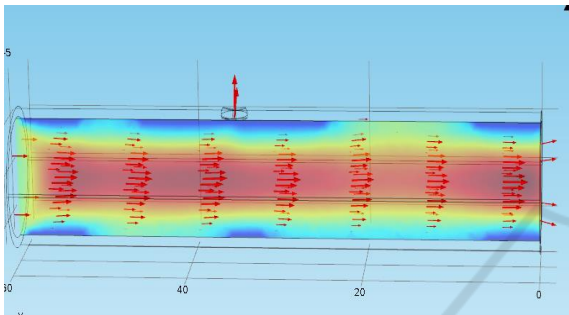


Figure 11: Hemorrhagic condition: Rupture at a weak point.

Figure 10 shows the blood flowing through the artery when no hemorrhage happens. The velocity of blood and the pressure inside the artery are measured as 0.24 m/s and 4.29 Pa, respectively. Figure 11, however, shows the hemorrhagic condition where the artery has been ruptured at that particular weak point. The velocity and the pressure, in this case, are measured to be as 0.22 m/s and 4.07 Pa, respectively. This change in pressure and velocity is the consequence of leakage of blood from the ruptured portion. This decrease aids in lowering of cerebral oxygenation level discussed later.

5 CLASSIFICATION OF ISCHEMIC AND HEMORRHAGIC STROKE USING NIRS SIMULATION

Using Helmholtz equations option in COMSOL Multiphysics, a point light source has been created in the same previous model just above the artery with properties shown in Table VI so that its absorption and reflectance can be measured.

Figure 12 shows the modeling of near infrared radiation source positioned above the artery which is used for transmitting NIR radiation into the artery.

Table 6: Optical properties of artery.

Diffusion coefficient (D)	3.17×10^{-4}
Absorption Coefficient (1/m)	50
Boundary Impedance	0.182

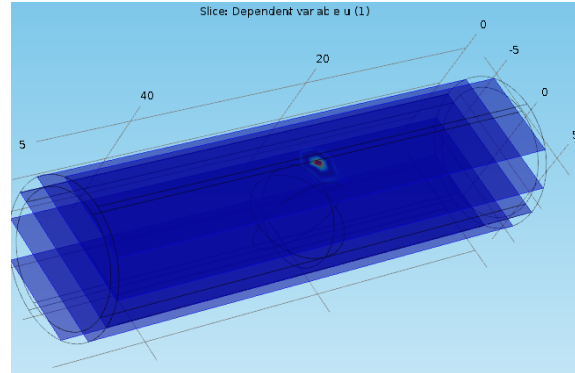


Figure 12: Location of light source just above the artery.

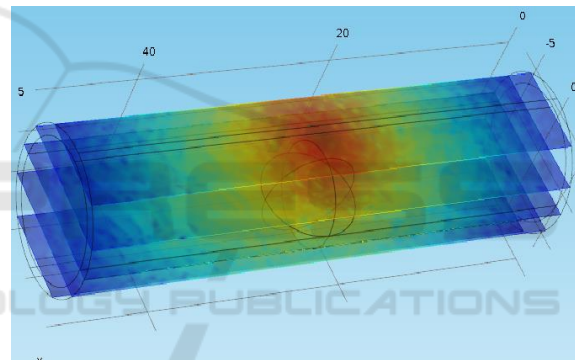


Figure 13: Pattern of penetration of light into the artery.

The pattern of the radiation distribution is shown in Figure 13, which is intense at the point source and gradual decreases in the regions away from the point source.

In order to see the relation between the varying size of the blockage and the boundary flux which is a direct measure of absorbance, the spherical blockage has been varied, and the boundary flux has been measured against every value.

The 6mm radius of blockage shows the ischemic condition, against which the values of boundary flux have been measured as shown in Table VII and Figure 14.

The above graph shows the absorption value decay as the blockage increases up to the ischemic condition. The absorption in the case of the healthy artery is measured approximately as 20, and in the case of hemorrhage, it is measured approximately as 18.

Table 7: Relation between boundary flux and blockage radius.

Radius of blockage (mm)	Boundary flux (1/m)
3	19.27
3.5	19.12
4	18.95
4.5	18.76
5	18.55
5.5	18.32
6	18.07

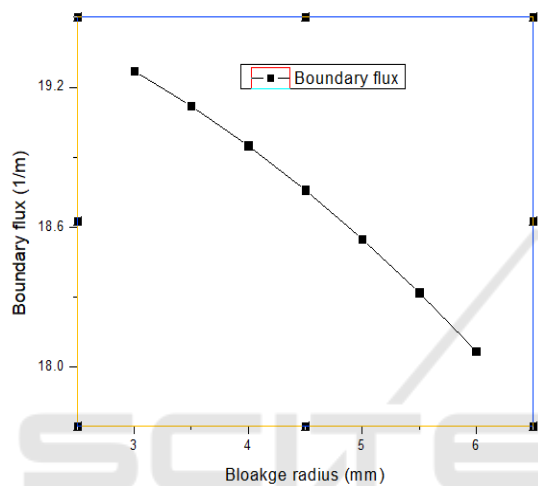


Figure 14: Graph showing boundary flux versus blockage radius.

Considering the proportionality of volumetric flow and absorption in the previous sections for both ischemic and hemorrhagic conditions, the cerebral oxygenation level is plotted against time as shown in Figure 15.

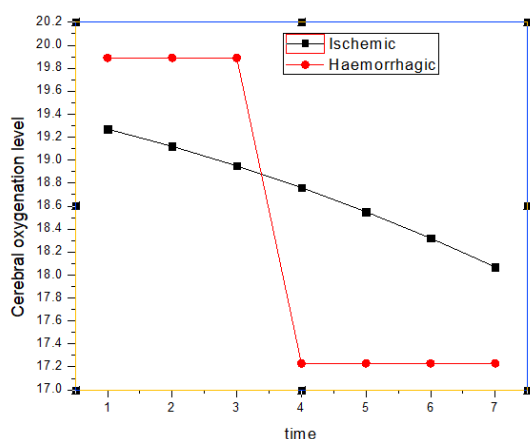


Figure 15: Change in cerebral oxygenation level for the ischemic and hemorrhagic condition.

Figure 15 shows the change in cerebral oxygenation level, which is considered proportional to the absorption in table VII, which has been plotted against time, here time is considered proportional to the continuous increase of the plaque formation in the artery.

6 CONCLUSION

In this paper, an approach of classification of ischemic and hemorrhagic strokes, based on near infrared spectroscopy, has been studied. The blood flow velocity and the pressure profile in the artery containing blood clot and plaque have been plotted. The blood flow velocity for which hemorrhage occurs is found to be 0.22 m/s. The change in stiffness of the affected part of an artery due to plaque accumulation has also been discussed. Displacement and stress values against varying blood flow velocity have been found to be greater in case of the artery with plaque than the pure artery. The cerebral oxygenation level, which is proportional to volumetric flow rate and near infrared light absorption, has been found decaying with the increasing size of blockage with time. Further works are going on.

REFERENCES

- Pandian JD, Sudhan P. Stroke, 2013. Epidemiology and stroke Care Services in India. Journal of stroke.: 15(3):128-134.
- Kamalakaran S, Gudlavalleti ASV, Gudlavalleti VSM, Goenka S, Kuper H., 2017. Incidence and prevalence of stroke in India: A systematic review. The Indian Journal of Medical Research. 146(2):175-185.
- Banerjee TK, Das SK., 2016. Fifty years of stroke Research in India. Annals of Indian Academy of Neurology. 19 (1):1-8.
- Donnan GA, Fisher M, Macleod M, Davis SM. 2008. "Stroke." Lancet. 371(9624): 1612-23.
- Radic B., 2017. Diagnosis and Treatment of Carotid Artery Stenosis. J Neural Stroke 7(3): 00238.
- Salonen JT, Salonen R., 1991. "Ultrasonographically assessed Carotid morphology and the risk of coronary heart disease." Arterioscler Thromb 11:1245-49.
- Mancini GB, Dahlof B, Diez J, 2004; " Surrogate markers for cardiovascular disease": structural markers. Circulation 109: IV22-IV30.
- A. Garje, Y.G. Adhav, D. Bodas, 2015. " Design and Simulation of Blocked Blood vessel of early detection of heart disease" Proceedings of 2015 2nd International Symposium on Physics and Technology of Sensors, Pune India.
- J. Mazumdar 1992, *BiofluidMechanics*, [Rever Edge] N.J: World Scientific, Singapore.